

Lab on a Chip

Accepted Manuscript



This is an *Accepted Manuscript*, which has been through the Royal Society of Chemistry peer review process and has been accepted for publication.

Accepted Manuscripts are published online shortly after acceptance, before technical editing, formatting and proof reading. Using this free service, authors can make their results available to the community, in citable form, before we publish the edited article. We will replace this *Accepted Manuscript* with the edited and formatted *Advance Article* as soon as it is available.

You can find more information about *Accepted Manuscripts* in the [Information for Authors](#).

Please note that technical editing may introduce minor changes to the text and/or graphics, which may alter content. The journal's standard [Terms & Conditions](#) and the [Ethical guidelines](#) still apply. In no event shall the Royal Society of Chemistry be held responsible for any errors or omissions in this *Accepted Manuscript* or any consequences arising from the use of any information it contains.

A flexible microneedle array as low-voltage electroporation electrodes for *in vivo* DNA and siRNA delivery

Zewen Wei^{1‡}, Shuquan Zheng^{2‡}, Renxin Wang^{3,4}, Xiangli Bu¹, Huailei Ma¹, Yidi Wu², Ling Zhu¹, Zhiyuan Hu^{1*}, Zicai Liang^{2*}, and Zhihong Li^{3*}

1 National Center for Nanoscience and Technology, Beijing 100190, China

2 Institute of Molecular Medicine, Peking University, Beijing 100871, China

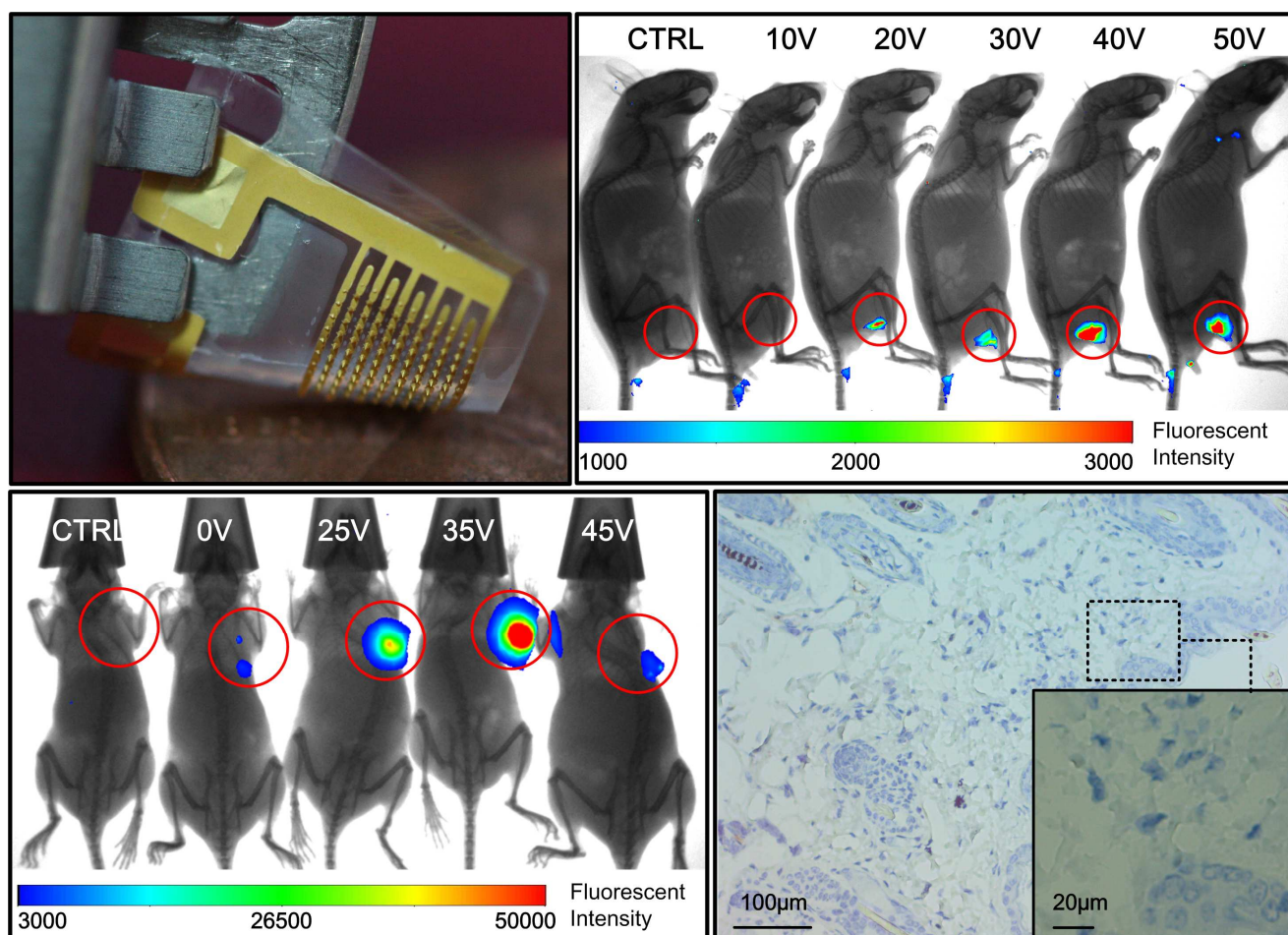
3 National Key Laboratory of Science and Technology on Micro/Nano Fabrication, Institute of Microelectronics, Peking University, Beijing 100871, China

4 Science and Technology on Electronic Test & Measurement Laboratory, Key Laboratory of Instrumentation Science and Dynamic Measurement, North University of China, Taiyuan, China

‡ These authors contributed equally to the work

* Authors for correspondence, Zhihong Li (Zhkli@ime.pku.edu.cn, Fax 86-10-62751789), Zicai Liang (Liangz@pku.edu.cn, Fax +86-10-62769862), or Zhiyuan Hu (Huzy@nanoctr.cn, Fax 86-10-82545643).

Graphical contents entry



A flexible microneedle array electrode chip for low-voltage electroporation with good tissue adaption, efficient nucleic acid delivery, and minimum damage.

Abstract

In vivo electroporation is an appealing method to deliver nucleic acid into living tissues, but the clinical application of such method was limited due to the severe tissue damage and the poor coverage of the tissue surface. Here we present the validation of a novel flexible microneedle array electrode chip (MNAE), in which the microneedle array and the flexible substrate are integrated together to simultaneously facilitate low-voltage electroporation and accomplish good coverage of tissue surface. The efficient delivery of both DNA and siRNA was demonstrated on mice. By penetrating the high-resistance stratum corneum, the electroporation voltage was reduced to about 35 V, which was generally recognized safe for human. Also, the first pathological analysis of microneedle-electroporated tissue was carried out to thoroughly access the skin damage which is an important consideration in pre-clinical studies of electroporation devices. This MNAE constitutes a novel way of *in vivo* delivery of siRNA and DNA to certain tissues or organs with satisfactory efficiency, good adaptation to tissue surface profile as well as minimum tissue damage, and thus avoiding the disadvantages of existing electroporation methodologies.

Keywords: Electroporation; siRNA delivery; Gene therapy; Flexible microneedle array.

1. Introduction

Nucleic biotherapeutics, such as DNA vaccination¹ or gene-based antitumor therapy², have been greatly expected by the public. However, difficulties in the delivery of DNA and siRNA into cells have prevented the development of nucleic therapeutics against many diseases^{3,4}. Nucleic acid carriers including viral vectors and chemical vectors have been proved effective for certain clinical applications⁵, albeit concerns about the safety issues of vectors⁶. There are, however, still many tissues and organs to which such vectors cannot get efficient access^{3,7,8}.

In vivo electroporation, as a non-vector physical technology, has been found to be a promising method to deliver DNA into animal tissues⁹. The first demonstration of *in vivo* electroporation was based on a hand-assembled dual-needle electrode¹⁰. Due to the operation convenience and no selectivity of tissue kinds, dual-needle electrode has been developed to a common used laboratory device for *in vivo* electroporation. However, the electric field generated by the dual-needle electrode is uneven. As a result it can only act on a small area of target tissues between two electrodes. A variety of strategies have exploited the needle matrix¹¹ and the modification of electrical parameters¹² or geometric size^{13, 14} to extend the range of tissue coverage. Unfortunately, the clinical application of conventionally machined and/or hand-assembled needle-based electroporation devices has been limited by another fatal defect, the severe tissue damage, induced by the high voltage and the needle penetration. Recently, benefited from the emerging microfabrication technology, some microneedle arrays were developed for transdermal drug delivery^{15,16} and *in vivo* electroporation^{17,18,19}. Theoretically, both the voltage and the penetration-induced damage could be remarkably reduced by shrinking the needle dimension and the space between needles to a few hundreds of microns. Yet the rigid substrate prevented the existing microneedle arrays from adapting the shape of different living tissues. Therefore it is fundamentally inappropriate for *in vivo* application. Largely because of this, the verification of DNA transfection utilizing microneedle array was only performed *in vitro*. To match the tissue profile, flexible substrates were also explored^{20,21}. In these reports, however, only planar electrodes were

placed on the flexible substrate. While utilizing planar electrodes, the high-resistance stratum corneum of skin prevented subcutaneous tissues from efficient electroporation with various degrees.

Despite all the new advances brought by the microfabrication technology, *in vivo* nucleic acid delivery by microneedle-array-based electroporation has not been conclusively proved. Besides, the tissue damages induced by the microneedle and/or the electric field have yet to be investigated. This study addresses these challenges with a novel strategy. We integrated microneedle array and flexible substrate together, forming an efficient electroporation electrode chip for *in vivo* nucleic acid delivery. The flexible substrate provided a close contact with living tissue, while the silicon microneedles penetrated the high-resistance stratum corneum and produced a sufficient electric field underneath the skin for electroporation. Using this flexible microneedle array, highly localized delivery of plasmid DNA (in healthy muscle tissue) and siRNA (into tumor) were both achieved on mice with high efficiency. Meanwhile, the electroporation voltage was reduced to about 35 V. Furthermore, the electric-induced skin damage induced by microneedle array was pathologically determined for the first time and full tissue recovery could be accomplished in less than 10 days.

2. Materials and methods

2.1. Materials

A RFP (pmRFP-C1) plasmid which encodes red fluorescence protein was used to determine the transfection efficiency of electroporation *in vivo*. RFP plasmid was purified using a commercial kit (EndoFree Plasmid Maxi Kit, TIANGEN, China). The sequence of Cy5-labelled siRNA (Ribo Co., China) is: sense: 5'-Cy5-CCUUGAGGCAUACUUCAAAdTdT-3'; antisense: 5'-UUUGAAGUAUGCCUCAAGGdTdT-3'. It was stabilized with certain chemical modifications and with a Cy5 fluorophore on the 5' of the sense strand. Optimal cutting temperature (OCT) compound (Sakura Finetek Inc., USA) was used for frozen section sample embedding. DAPI (4',6-diamidino-2-phenylindole, Zhongshan Goldenbridge, China) was employed for nucleus staining. Fluorescein isothiocyanate-labelled phalloidin for cytoskeleton staining (by staining F actin) and hyaluronidase for local injection were both supplied by Sigma-Aldrich, USA. Dulbecco's Modified Eagle's Medium (DMEM), fetal bovine serum (FBS), penicillin-streptomycin and trypsin were from Life Technologies, USA. Matrigel membrane matrix (Vigorous Inc., China) was utilized for subcutaneous tumor inoculation.

2.2. Cell lines and culture

For *in vitro* electroporation, HEK-293a, Hela and MDCK cells were grown in Dulbecco's modified Eagle's medium (DMEM) supplemented with 10% fetal bovine serum, 100 units/ml penicillin and 100 µg/ml streptomycin. Cells were incubated at 37°C in 5% CO₂ humidified atmosphere. To inoculate subcutaneous tumor, breast carcinoma cell line MCF-7 was purchased from the Cell Resource Center of Peking Union Medical College (Beijing, China). MCF-7 cells were cultured in DMEM which was supplemented with 10% fetal bovine serum, 100 units/ml penicillin and 100 µg/ml streptomycin and incubated at 37°C in humid atmosphere containing 5% CO₂.

2.3. Animals

Male C57BL/6 mice (age 6-8weeks) and female BALB/c nude mice (weighing 18-22g) for muscle and tumor electroporation were purchased from Vital River Laboratories (Beijing, China). Animals were maintained in Peking University Laboratory Animal Center, which is an AAALAC-accredited and specific pathogen free (SPF) experimental animal facility. All of the experimental animals in our study were treated in accordance with protocols approved by the Institutional Animal Care and Use Committee of Peking University.

2.4. Myocyte electroporation in C57BL/6

To electroporate the myocytes, C57BL/6 mice were anesthetized with pentobarbital sodium (i.p., 50 mg/kg) and the thighs were depilated carefully with blade. When intramuscular injecting, the syringe was stabbed into the muscle of the mouse thigh with 3-5 mm depth beneath the skin, and 40 μ l (1 μ g/ μ l) hyaluronidase was injected into muscle slowly. The hyaluronidase would diffuse in an area of 0.8-1.0 cm^2 . 30 minutes later, 40 μ l RFP plasmid (1 μ g/ μ l) was injected into muscle at the same area. 10 minutes later, MNAE was inserted to the skin of this area, then, 5 electric pulses of different voltages, provided by a pulse generator (ECM 830, BTX, USA), were applied for electroporation. The pulse duration was 20 ms, and the pulse interval was 2 s. No pulses were applied to the negative controls. All mice were detected for the RFP signal in the thigh muscle forty-eight hours after electroporation using an In-Vivo Imaging System (Carestream In-Vivo Imaging System FX Pro, Carestream Health, USA).

2.5. Evaluation of RFP expression in mouse myocytes

To determine the site of RFP expression, the muscle tissues were embedded in optimal cutting temperature (OCT) compound for frozen section after the whole-body imaging. Then the tissues in OCT compound were cut into 20 μ m pieces from epidermis to muscle, by freezing microtome (CM1510, Leica, Germany). Every 10 consecutive pieces were collected together to detect RFP signals with a microplate reader (Synergy Mx, BioTek, USA). 550nm excitation and 600nm emission were used to detect the signal intensity of RFP from muscle frozen sections.

2.6. Tumor electroporation and frozen section observation

For tumor electroporation assay, 5×10^6 MCF-7 cells were injected subcutaneously into the right axillary fossa of the BALB/c nude mice. The tumor-bearing mice were used for electroporation when the tumor volume was around 500 mm^3 . Tumor-bearing mice were divided into five groups. Group 1 was used as blank control; while the four other groups (group 2 to 5) were injected with $40 \mu\text{l}$ ($1 \mu\text{g}/\mu\text{l}$) hyaluronidase and $40 \mu\text{l}$ ($1 \mu\text{g}/\mu\text{l}$) Cy5-labelled siRNA intratumorally. The mice of group 2 to 5 were electroporated with the same way described in section 2.4. The voltages were 0V, 25V, 35V and 45V, respectively. All mice were examined for the Cy5 signal at 1, 2, 3, 4, 6, 10, 14 days after electroporation. To analyse the distribution of Cy5-labelled siRNA in MCF-7 tumor cells, ninety-six hours after electroporation, one tumor from each group was isolated from the animals and embedded in OCT, then got frozen by liquid nitrogen. The specimens were cut into $6 \mu\text{m}$ sections with frozen section equipment (CM1510, Leica, Germany). Then, all the sections were stained by DAPI for nucleus and by FITC-labelled phalloidin for F-actin (so that the nucleus and cell outline were displayed as blue and green when excited by certain fluorescence). Finally, all slides were examined under the confocal microscope (LSM710, Zeiss, Germany).

2.7. Immunohistochemistry

Skin tissues were fixed in 10% formalin for twenty-four hours. Tissues were processed for routine histopathological examination: dehydrated sequentially in 50%, 70%, 80%, 95%, and 100% ethanol, embedded in paraffin, cut into $5 \mu\text{m}$ thick histologic sections with a microtome (CM1900, Leica, Germany). For the immunohistochemistry of LCA (lymphocytotoxic activity) in lymphocytes, paraffin of sections was removed with xylene for 5 minutes 2 times, then the slides were equilibrated in Tris-buffered saline (TBS) for 5 minutes 3 times. Microwave-mediated antigen retrieval was performed using a microwave oven. Slides were incubated for 1 hour at room temperature in TBS containing 2% (w/v) normal goat serum for blocking nonspecific binding. Incubation with primary antibodies (rabbit anti mouse LCA antibody, 1:200) was carried out in a humidified chamber overnight at 4°C . Then, the slides were rinsed with PBS for 5 minutes 3 times and incubated for 2

hours at room temperature with secondary antibody (goat anti-rabbit IgG labelled with HRP), and then washed 3 times in PBS. After the DAB (DK-2600, Glostrup, Denmark) staining, all the slides were counterstained with hematoxylin and dehydrated. Treatment without the primary antibody was used as the negative control. Micrographs were taken by microscope system (BX51, Olympus, Japan). Then, the images were analysed with an image software (ImageJ from NIH) to count the lymphocytes in sections.

3. Results and discussions

3.1. Design and fabrication of the flexible microneedle array electrode

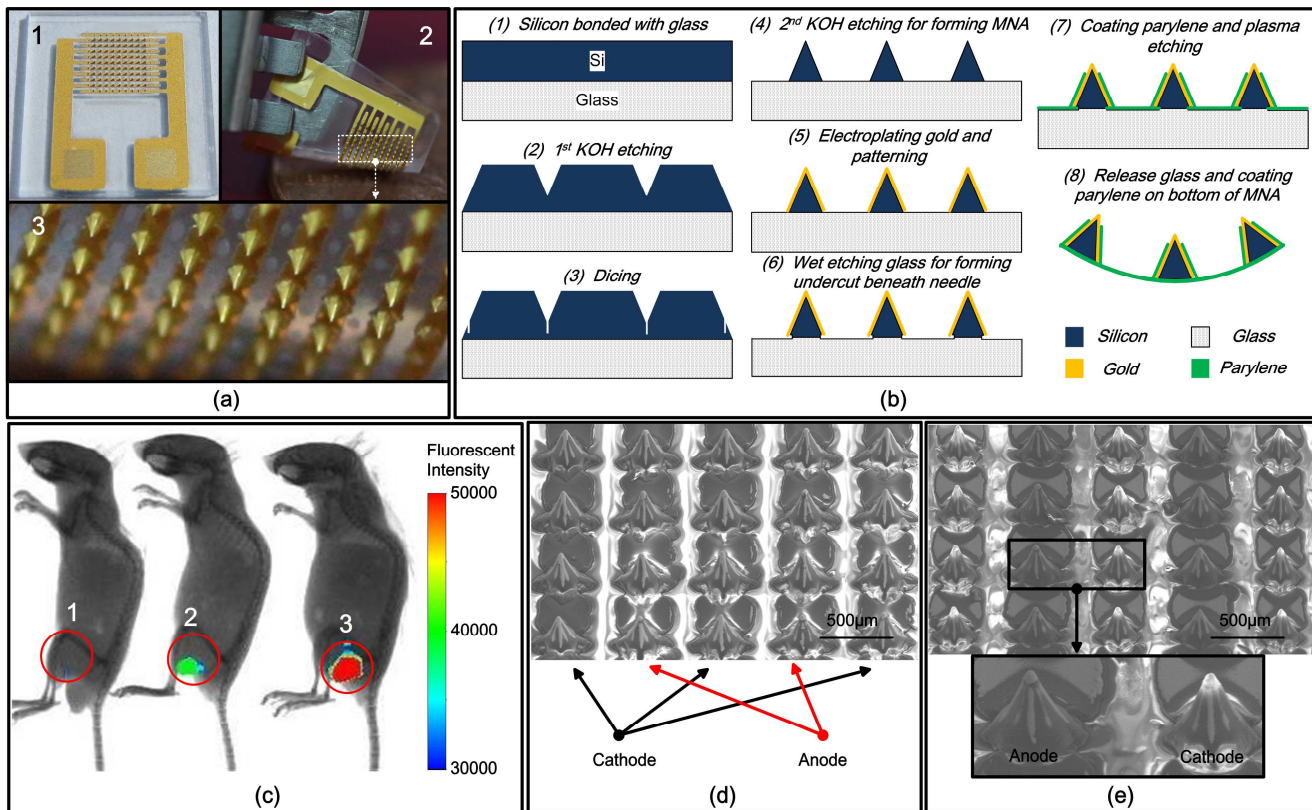


Figure 1. The flexible microneedle array electrode chip (MNAE) and its skin insertion test.

(a), the photos of MNAE, 1, the MNAE attached with the glass substrate, 2, the flexibility of MNAE, 3, the close-up view of silicon microneedles coated with gold. (b), the fabrication process of MNAE. (c), the skin insertion test of MNAE, after dropping a drop of Cy-5 labeled siRNA on un-haired skin of mice leg, the MNAE was inserted into skin once (2) or five times (3), while the control mouse (1) was pushed by a flat glass, then all three legs were washed thoroughly for 10 minutes before imaging. The MNAE insertion areas were labelled with red circle. The fluorescent image shows the siRNA sinks into the skin by MNAE penetration, and repetitive MNAE penetration increases the amounts of siRNA in the skin. The SEM photos of MNAE before (d) and after (e) skin penetration and electroporation show no needle damage but small changes on surface appearance of cathode.

The flexible microneedle array electrode (MNAE) chip was designed for the low-voltage electroporation of tissue underneath the skin. In order to accomplish this goal, the MNAE should be pliable to fit the different tissue surface profile as well as mechanically strong enough to penetrate the stratum corneum. Besides, the MNAE should be capable to withstand the high electric field for electroporation. To fulfil these requirements, a transparent parylene film was used as substrate for electrodes due to its good flexibility. It provides a tight contact between MNAE and living tissues with different surface profiles. The parylene layer also acts as insulator between

electrodes. Silicon was chosen as the material of the microneedle due to its good strength and compatibility with microfabrication technology. Gold was employed as the material of electrodes because of its good conductivity and bio-compatibility. The prototype of MNAE is shown in Figure 1a, 81 microneedles were coated and parallel connected by gold, forming a rectangle interdigital electrodes array. The height of microneedle was 190 μm , and the spacing between microneedles was 340 μm . The effective area of the MNAE was designed to about 20 mm^2 to fit the typical size of tumor and muscle tissue of experimental mice. To penetrate the high-resistance stratum corneum, the height of microneedles should be designed larger than the thickness of the stratum corneum. The height of microneedles also decides how deep the effective electrical field could reach. Once the height of microneedles was selected, the applied voltage could be reduced by shrinking the spacing between microneedles. Besides, shrinking the spacing meant increasing the density of microneedles in a certain area. Consequently, the uniformity of electric field could also be improved. Therefore, better electroporation efficiency, along with lower tissue damage, could be expected. To sum up, the height of microneedle depends on the target tissue depth, and the smaller space between microneedles could theoretically be beneficial to electroporation performance. By redesigning the layout for lithography, the MNAE size can be easily varied according to the needs of different applications.

The MNAE was fabricated with MEMS (Micro-electro-mechanical system) processes, including sputtering, dicing, lithography, electroplating and wet etching. The basic fabrication process was briefly reported²² and in detail shown in Figure 1b and supplementary Figure S1. Briefly, a silicon wafer, bonded with glass, was wet etched twice to form silicon microneedles. Silicon dicing was employed to limit the interval between microneedles. A gold layer was sputtered to coat the microneedles and patterned as electrodes. To withstand the strong electroporation current, electroplating was employed to thicken Au layer to 6 μm . Standard BHF (buffered hydrofluoride acid) solution was used to etch glass for 8 μm to form an undercut beneath the microneedles. Using PDS2010 system (Specialty Coating System, USA), a parylene C film (8 μm) was coated on the top side of microneedles. The gold electrodes were then exposed by plasma etching of the

polyethylene film. After releasing the flexible microneedles from the glass substrate, another polyethylene layer (2 μm) was coated to encapsulate the bottom of microneedles, finally forming the MNAE.

3.2. Skin insertion test

We firstly tested the mechanical strength of the MNAE. The Cy-5 labelled siRNA, to which the skin is impermeable, was placed on un-haired leg skin of three individual mice. Then we pushed the MNAE into the skin of two mice, while the third mouse was treated with a flat glass. 10 minutes later, the skin was thoroughly washed and fluorescently imaged. As shown in Figure 1c, only one time MNAE insertion makes the siRNA soak in the skin (mouse No. 2), while repeatedly insertion of MNAE makes the skin more permeable to siRNA (mouse No. 3). As contrast, the mouse skin treated with flat glass (mouse No. 1) maintained impermeable to siRNA. Besides, the fluorescent area shows uniform fluorescent intensity, which indicates the flexible MNAE chips adapt the tissue profile. Using scanning electron microscope (SEM), we then imaged the MNAE before and after skin penetration and subsequent electroporation to determine whether the needle broke happened. As shown in figure 1d and 1e, the MNAE maintained its profile and strength. For the entire MNAE chip, no microneedle damage was observed. The gold layer also withstood the high current and kept intact on microneedles. Therefore, the potential biological hazard related to MNAE cracking in tissue could be avoided. Above results indicated that the MNAE adapted the skin profile, penetrated the skin and maintained its integrity after insertion and electroporation.

3.3. DNA transfection

One prominent feature of the MNAE is the integration of microneedle electrodes and flexible substrate. Compared with previous microneedle electrodes with rigid substrate^{18,19}, the flexibility of MNAE (Figure 1a) enables the adaptation to different tissue surface profile, providing uniform electroporation efficiency over the whole effective area of MNAE. In contrast to previously reported flexible electroporation chip integrating planar electrodes^{20,21}, the MNAE holds the capability to penetrate the high-resistance stratum corneum and produce a sufficient electric field beneath the skin under a low voltage. To determine the voltage required for sufficient electric field, COMSOL

ver 3.5a was used to simulate the electric field distribution of MNAE (Figure 2a) and previous planar electrodes (PE, Figure 2b). The simulation reveals that the avoidance of electric field consumption on skin remarkably reduced the electroporation voltage. Utilizing MNAE, 25 V would produce an electric field stronger than that was produced by 70 V with PE, in the depth range from 100 μm to 700 μm beneath the skin (Figure 2c).

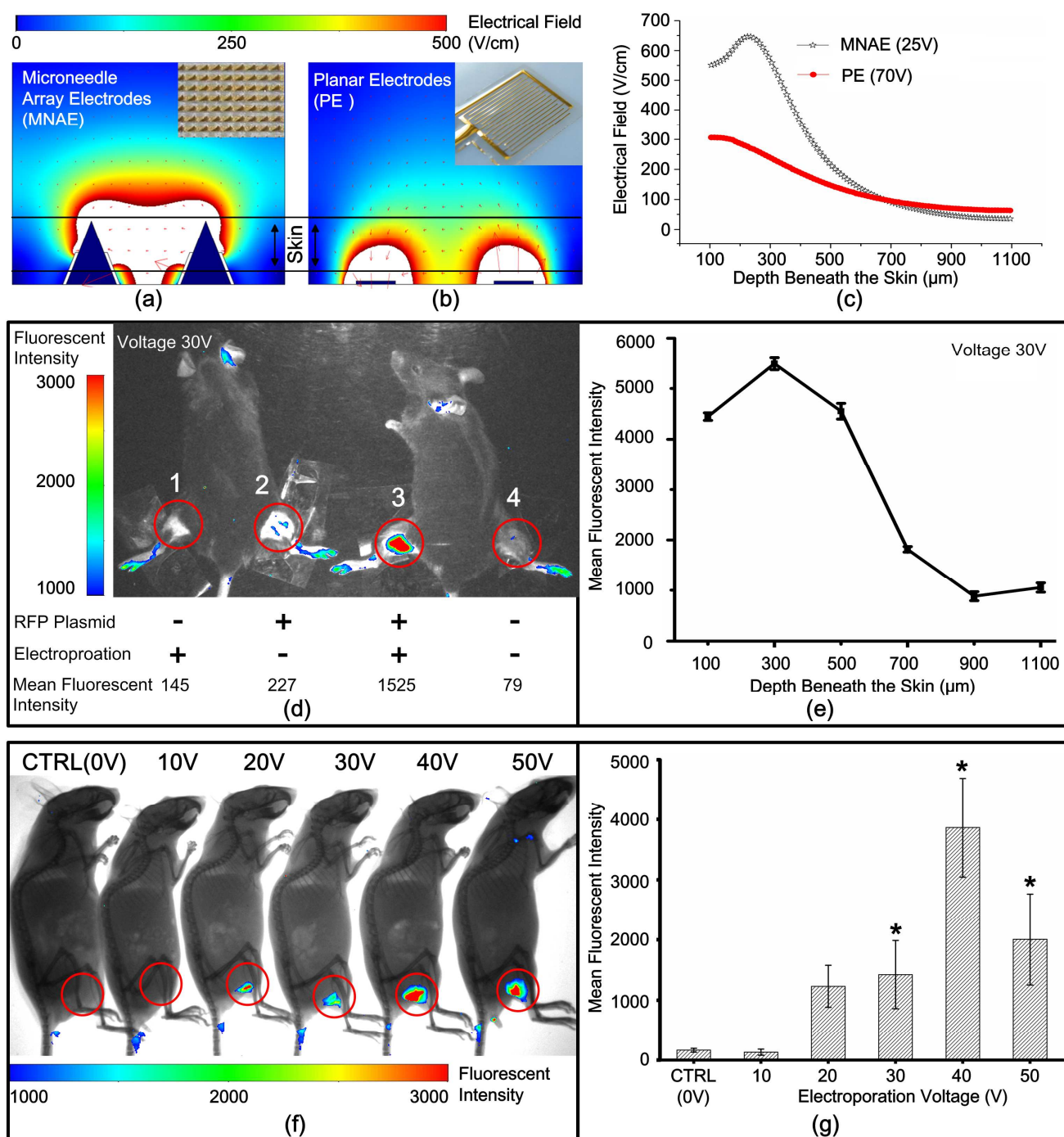


Figure 2. Electric field simulation and DNA transfection of MNAE

(a) and (b), the simulation of electric field generated by microneedle array electrodes (MNAE) and planar electrodes (PE). (c), the simulation of the relationship between the electric field strength and the depth beneath the skin. Compared with PE, MNAE could produce stronger electrical field beneath the skin with lower voltage. (d), the whole body fluorescent images of 4 mice whose leg muscle tissues received the following treatment: 1, with electroporation, but without RFP plasmid injection; 2, with RFP plasmid injection, but without electroporation; 3, with both RFP plasmid injection and electroporation; 4, without treatment, as negative control. The electroporation voltage was 30 V. Fluorescent images were merged with visible-light images to monitor the physical integrity of mouse skin. (e), the quantitative analysis of the mean fluorescent intensities of muscle frozen sections of different depth beneath the skin. The muscle was injected with RFP plasmid and electroporated under 30 V. Data were the average of three exposures. Each data was showed as the mean \pm S.D. (f), the whole body fluorescence intensity image of the mouse as control (only with the injection of hyaluronidase) and other 5 mice treated with the same RFP plasmid injection and different electroporation voltages. (g), graphical representation of mean fluorescence intensity as a function of electroporation voltage. * $P < 0.05$ vs control mice (voltage 0 V). Data were the average of three independent assays. Each data was showed as the mean \pm S.D. In (d) and (f), the electroporated areas were labelled with red circles.

The high electroporation efficiency of MNAE was firstly verified by *in vitro* transfection of plasmid DNA (supplementary Figure S2). Data suggested high transfection efficiencies (65% to 80%) were achieved for GFP plasmid transfection, and electroporated cells were proliferating well, maintaining ideal viability.

Muscle is a widely used and very important tissue for *in vivo* DNA transfection study. RFP plasmid was employed to investigate the capability of MNAE for *in vivo* DNA transfection since the tissue-penetration capacity of near-infrared (NIR) fluorophores (eg. RFP) are superior to those with shorter wavelength (eg. GFP)²³. As shown in Figure 2d, all four legs of two mice were sequentially numbered for the assay. All four legs were firstly injected with hyaluronidase which was reported capable of increasing tissue permeability and enhancing the transfection efficiency of plasmid DNA when used in conjunction with electroporation²⁴. Then mouse legs received following treatments respectively: 1, with electroporation, but without RFP plasmid injection; 2, with RFP plasmid injection, but without electroporation; 3, with both RFP plasmid injection and electroporation; 4, without treatment, as negative control. The detailed electroporation procedures were described in section 2.4. Forty-eight hours after electroporation, leg 3 showed obvious and even-distributed fluorescence, hinting efficient and even expression of RFP plasmid, while other three legs exhibited no fluorescence. It is observed that the fluorescent area on leg 3 and the

effective MNAE area are approximately equal. It indicates the MNAE closely fitted the profile of mouse leg. By checking the visible-light images, the integrity of skin after electroporation was confirmed. Also, the comparison test of DNA transfection efficiency on MNAE, dual-needle electrodes (DNE) and flexible planar electrodes (PE) was also finished using the similar electroporation procedures (supplementary Figure S3). The results demonstrate that the MNAE remarkably reduced the electroporation voltage (DNE, 240V; PE, 70V; MNAE, 30V) and acquired the similar DNA transfection with those DNE and PE did.

We then analysed the DNA transfection efficiency in different tissue depth. The muscle tissues were frozen sectioned forty-eight hours after electroporation, and then mean fluorescent intensities (MFIs) of different sections were quantitatively analysed. The results (Figure 2e) reveal that the relationship between MFI (representing transfection efficiency) and depth beneath the skin fits the simulation results of the electric field distribution (Figure 2c). Meanwhile, the section analysis also suggests that the effective depth of low-voltage (30 V) electroporation could reach up to 700 μm , which is enough for many nucleic biotherapeutics, such as DNA vaccination and treatment of near-skin tumor or other subcutaneous tissue.

One of the main obstacles limiting *in vivo* electroporation from clinical application is the unsafe voltage. To determine the optimized voltage for efficient DNA transfection, the MFI under different voltage were quantitatively analysed. As shown in Figure 2f and 2g, the MFI increases with the rise of voltage before reaching its peak value while the voltage is 40 V. A higher voltage results in the decrease of MFI, which implies the damage of tissue cells probably affected the DNA expression,

3.4. siRNA transfection

RNAi has become an important technology for manipulating cellular phenotypes, understanding gene functions, and more importantly, ablating tumor²⁵. However, considering that the naked siRNA would be easily eliminated by circulation, the carrier was so far necessary for siRNA-based

therapy, albeit the safety concerns. Differing from systematic carrier-based delivery, electroporation is a localized method, enabling high target specificity and satisfactory bioavailability of siRNA. Therefore, *in vivo* electroporation has the potential to become a promising siRNA delivery strategy. However, efficient siRNA delivery using microneedle-based electroporation, to the best of our knowledge, has yet to be conclusively demonstrated.

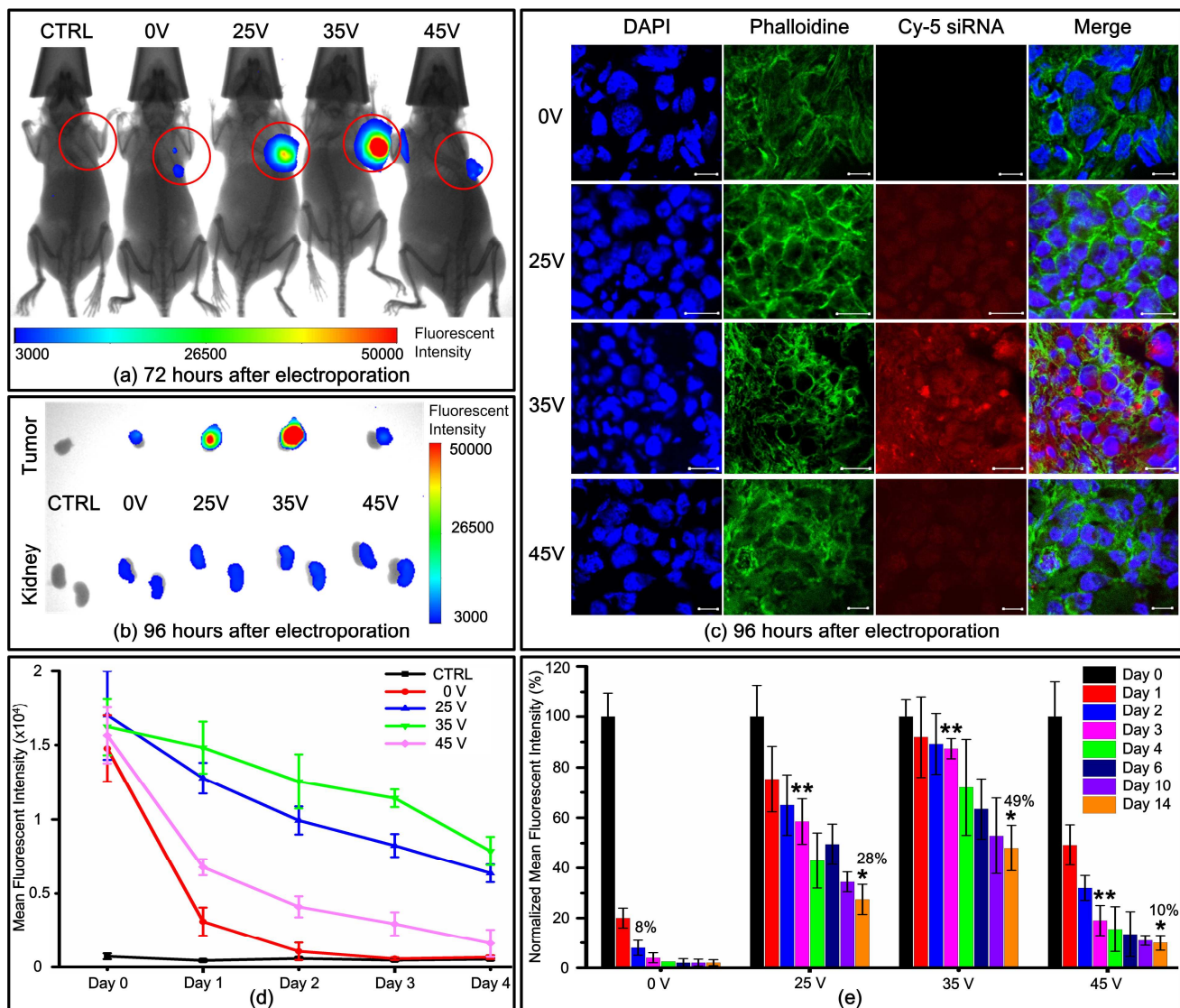


Figure 3. siRNA transfection by MNAE

(a), the whole body fluorescent images of 5 MCF-7 tumor-bearing mice received the following treatment: the leftmost mouse as control, without neither Cy-5 labelled siRNA injection nor electroperoration; the second left mouse, with Cy-5 labelled siRNA injection but without electroperoration; the other three mice, with the same amount of Cy-5 labelled siRNA injection and electroperoration under different voltages (25 V, 35 V, 45 V). The electroperated areas were labelled with red circles. (b), the fluorescent images of MCF-7 tumors and kidneys from sacrificed mice treated with the same conditions as (a). (c), Confocal laser scanning microscopy (CLSM) images of frozen sections of MCF-7 tumor tissues. Tumor with Cy5-labeled siRNA injection but without

*electroporation showed no fluorescent signal (uppermost panel). Tumors received injection of Cy5-labeled siRNA and electroporation exhibited significant fluorescence (lower three panels), in which the nuclei were stained by DAPI (blue), and the F-actin was stained by FITC-labeled phalloidin (green), to highlight the rough cell outline. The tumor electroporated under 35 V showed the strongest fluorescent intensity, in which the Cy5-labeled siRNA distributed around the nuclei and F-actin staining further confirmed the siRNA stayed in cytoplasm. (d), graphical representation of mean fluorescence intensity as a function of time after electroporation, in which the same grouping method described in (a) was used. (e), the relationship between mean fluorescence intensity and time after electroporation was studied in a prolonged time (14 days). The mice treated with siRNA injection but without electroporation (0 V) were used as control. For each group, the mean value before treatment was as benchmark (100%), the value post-treatment was normalized to the benchmark. * $P < 0.01$ and ** $P < 0.05$ vs control mice (voltage 0 V). In (d) and (e), data were the average of three independent assays, each data was showed as the mean \pm S.D., day 0 means right before electroporation, day 1 means 24 hours after electroporation, and so on.*

A xenografted subcutaneous tumor model was deployed to assess the capability of MNAE to deliver siRNA. Compared with muscle, tumor is with more irregular surface profiles which makes conventional dual-needle electrodes inefficient for good coverage. Using protocols described in section 2.6, we investigated the delivery of Cy5-labelled siRNA into tumors. Figure 3a shows the whole body fluorescent image of tumor-bearing mice which were treated with escalating voltages. For unelectroporated (0 V) mouse, the tumor fluorescence was very weak, which means the majority of injected Cy5-labelled siRNA was eliminated by circulation. As a contrast, the tumors which were electroporated with 25 V or 35 V showed significant fluorescence. It demonstrated that the MNAE did facilitate the siRNA delivery into tumor cells, slowing down the siRNA elimination. The tumor electroporated with 35 V showed a higher fluorescent intensity (indicating better siRNA delivery) than which was observed on the mouse treated with 25 V. Similar with what happened in muscle electroporation, a higher voltage (45 V) decreased the tumor fluorescence, hinting the worsening of electroporation efficiency. For acquiring a clear observation, the mice were sacrificed ninety-six hours after electroporation. The tumor and the kidney were fluorescently imaged (Figure 3b), the tumors showed a similar fluorescence vs voltage relationship with what was observed in the whole body image. The accumulation of siRNA in tumor was reconfirmed by the low fluorescent intensity in kidneys. Besides, the constant fluorescent intensity in kidneys hints a stable siRNA elimination process. To further confirm the subcellular distribution of Cy5-labelled siRNA in tumor cells, the tumor was frozen sectioned, stained, and imaged by confocal microscopy ninety-six hours after electroporation (Figure 3c). In unelectroporated tumor cells (0 V),

no fluorescent siRNAs was observed. In electroporated tumor cells (25 V, 35 V and 45 V), significant levels of siRNAs remained inside of the cells. By the image analysis, we found that the highest transfect efficiency was achieved under 35 V, which confirms 35 V as optimized voltage for efficient siRNA transfection.

For tumor therapy, a certain amount of siRNA in the cells was required. Therefore, the slower the siRNA amount decreases, the better the treatment effect is^{25,26}. To study the decrease of siRNA after electroporation, the fluorescent intensities of tumors were quantified for consecutive 4 days. As shown in Figure 3d, at day 0 (right before electroporation), all 4 tumors injected with the same amount of siRNA exhibited similar mean fluorescent intensity (MFI), since the MFI represented the amount of siRNA. For all 4 siRNA-injected tumors, the MFI decreased as time went on. For the unelectroporated tumor, a dramatic drop of MFI was observed at day 1. Meanwhile, the tumor treated with 35 V electroporation maintained the highest MFI at all images of 4 consecutive days, which indicated the 35 V was the optimized voltage for maintaining siRNA amount in cell interiors. To further study the decreasing of siRNA amount, the MFIs of 4 siRNA-injected tumors were monitored for a prolonged period (14 days). The unelectroporated tumor (0 V) was considered as negative control. As shown in Figure 3e, at the day 14, 49% of siRNA remained in the tumor treated with 35 V electroporation, while the numbers for tumors treated with 25 V and 45 V were 28% and 10%, respectively. The results reveal that the treatment cycle could be prolonged to 14 days, since 49% siRNA remaining is high enough to meet the requirement of siRNA-based tumor therapy^{25,27}.

Overall, the MNAE electroporation facilitates the efficient siRNA delivery to tumor cells, and the optimized voltage is 35 V. Moreover, a high amount of siRNA could still be observed in tumors even 14 days after electroporation.

3.5. Skin damage evaluation

Tissue damage was the main concern that prevented needle-based electroporation devices from clinical applications. For conventional machined and/or hand-assembled needle-based devices, the trauma caused by high voltage and needle invasion could be easily monitored by visual examination of skin appearance. For micromachined devices, the applied voltage was reduced to less than 100 V by shrinking the spacing between electrodes. Thus the electroporation process probably did not appear to significantly affect skin appearance, and such devices were usually considered biologically safe under this circumstance. However, in pre-clinical studies, the trauma-induced infection should be considered as a more important issue for tissue health, even when no skin damage was found by visual check. To thoroughly evaluate the effect of MNAE electroporation on skin damage, LCA (lymphocytotoxic activity), which was one of the gold standards to analyse the tissue infection in pathology²⁸, was employed to assess the lymphocytic infiltration of histologic sections from electroporated skin tissue. As shown in Figure 4a, the skin tissue exhibited recognizable lymphocytic infiltration twenty-four hours after electroporation. As shown in Figure 4 b, a reduced lymphocytic infiltration was observed seventy-two hours after electroporation, hinting the recovery of damaged tissue. As shown in Figure 4c, the lymphocytic infiltration was observed fully healed 10 days after electroporation. The lymphocytic infiltration ratios were further quantified to determine the relationship between applied voltage and tissue infection (Figure 4d). A flexible microchip with planar electrodes (PE, described in Figure 2b) was introduced for comparison. For MNAE, the lymphocytic infiltration ratio increased as the voltage raised. Under the same voltage (45 V), MNAE and PE induced similar lymphocytic infiltration. However, the minimum effective voltage for PE is 70V, with which significantly increased lymphocytic infiltration ratio was observed. The lymphocytic infiltration would get worse if one raised the applied voltage to 90 V for better electroporation efficiency. The results reveal that for micro-scaled electrodes, either planar or microneedle-based, the applied voltage was the key factor for tissue damage.

In fact, the majority of gene-based biotherapies require periodic treatments^{1,2}. Under this circumstance, the tissue damage induced by the first treatment should be fully recovered before the

second treatment. To further understand the healing process of the tissue infection, the lymphocytic infiltrations of skin tissues electroporated by 25 V, 35 V and 45 V were monitored for a long period (10 days). As shown in Figure 4e, as the voltage increased, the lymphocytic infiltration aggravated. For the voltage of 45V, it cost 10 days for the full recovery of tissue, while the voltages of 35 V and 25 V cost 8 days and 4 days, respectively. Considering the treatment cycle of siRNA delivery could be prolonged to 14 days, as described in section 3.4. The recovery time is enough for an ideal tissue healing.

Taken together, the skin tissue damage was proved to be related to electroporation voltages. For MNAE-based electroporation, full tissue recovery could be accomplished in less than 10 days.

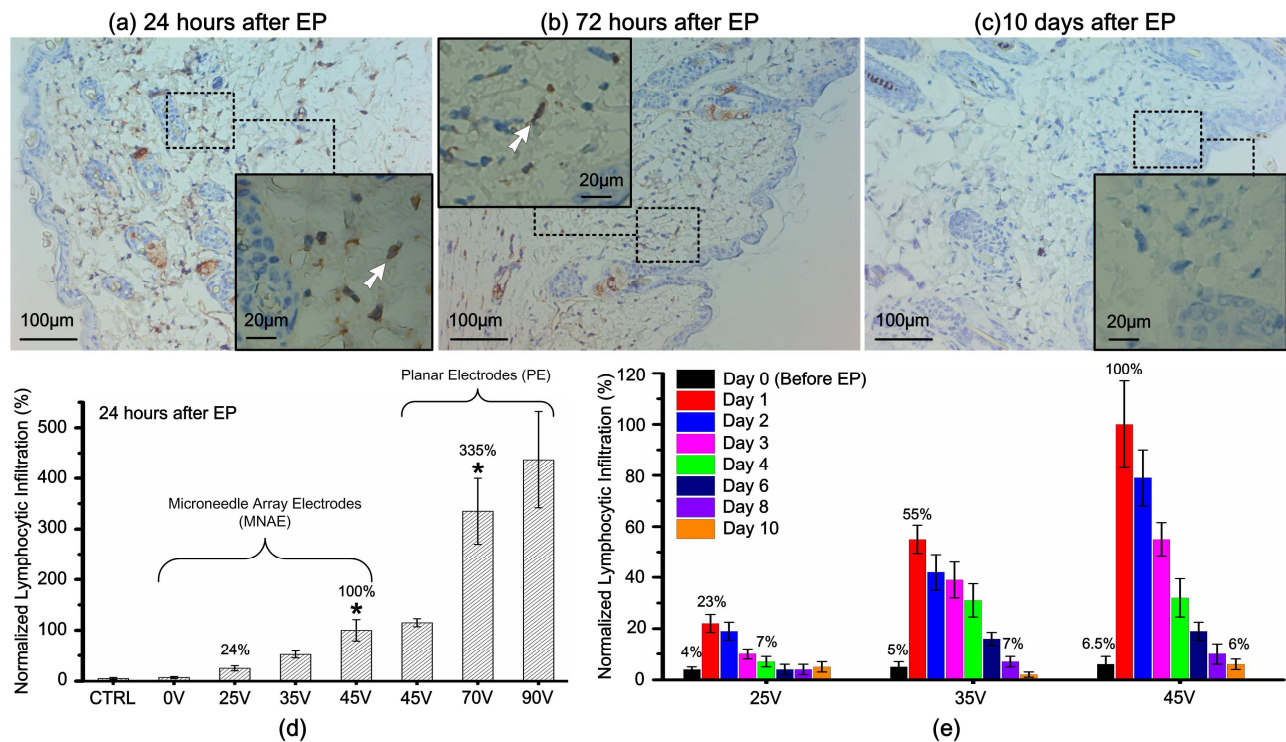


Figure 4. Evaluation of skin tissue damage induced by MNAE electroporation

The images of sections from the skin tissues 24 hours (a), 72 hours (b) and 10 days (c) after electroporation. The LCA was employed to indicate the lymphocyte (brown spots indicated by white arrows). (d), by quantitatively analysing the section images (using Image J from NIH) 24 hours after electroporation, the relationship between lymphocytic infiltration ratio and applied voltage was accessed. * $P < 0.01$ vs mice treated with 0 V. (e), to evaluate the tissue damage recovery, the lymphocytic infiltration of skin tissues electroporated by 25 V, 35 V and 45 V was monitored for 10 days. In (d) and (e), the mean value of the tissue image 24 hours after electroporation by 45 V was used as benchmark (100%), all data were the average of three independent assays and normalized to the benchmark. data, each data was showed as the mean \pm S.D., day 0 means right before electroporation, day 1 means 24 hours after electroporation, and so on.

4. Conclusion

In vivo electroporation has been demonstrated to be a promising non-vector method to deliver DNA into cells of living tissues. The previous reported machined and/or hand-assembled needle-based devices were fundamentally inappropriate for clinical applications because of the severe tissue damage induced by high voltage and needle invasion. The emerging fabrication method of microneedle array offers the opportunity to realize *in vivo* nucleic acid delivery with low voltage and minimum tissue damage. This study advances this field in three ways. First, this paper presents a new strategy that integrates microneedle array and flexible substrate together to simultaneously facilitate low-voltage electroporation and good coverage of tissue surface. Second, for the first time, this paper provides tangible evidences of *in vivo* delivery of both DNA (to muscle) and siRNA (to tumor) utilizing microneedle-based electroporation. Also, the optimized voltage for efficient nucleic acid delivery was reduced to 35 V, which is generally recognized to be safe for human. Third, to thoroughly assess the skin damage, this study carried out the first pathological analysis of electroporated tissue which is quite necessary for pre-clinical studies. For micro-scaled electrodes, either planar or microneedle-based, the applied voltage is the key factor for lymphocytic infiltration which is the gold standard to evaluate trauma-induced tissue infection. By reducing the applied voltage to 35 V, the lymphocytic infiltration was significantly alleviated. Furthermore, the lymphocytic infiltration was also proved completely recoverable in a short period (about 8 days).

Overall, this study presents a flexible microneedle array electrode chip (MNAE) which enables efficient low-voltage electroporation and good coverage of tissue surface together. The high-efficiency nucleic acid delivery and minimum tissue damage were both verified on mice. The MNAE chip provides a promising means for highly localized, minimally invasive electroporation to deliver nucleic acid *in vivo* for gene therapy or DNA vaccination.

Acknowledgements

This work was supported by the National Natural Science Foundation of China (No. 61204118, 61176111 and 81273422), the National High Technology Research and Development Program of China (863) (No. 2012AA022501).

References

1. P. L. Lollini, F. Cavallo, P. Nanni and G. Forni, *Nature reviews. Cancer*, 2006, 6, 204-216.
2. I. M. Verma and N. Somia, *Nature*, 1997, 389, 239-242.
3. K. A. Whitehead, R. Langer and D. G. Anderson, *Nature reviews. Drug discovery*, 2009, 8, 129-138.
4. C. Scholz and E. Wagner, *Journal of controlled release : official journal of the Controlled Release Society*, 2012, 161, 554-565.
5. J. C. Burnett, J. J. Rossi and K. Tiemann, *Biotechnology journal*, 2011, 6, 1130-1146.
6. C. E. Thomas, A. Ehrhardt and M. A. Kay, *Nature reviews. Genetics*, 2003, 4, 346-358.
7. R. Kanasty, J. R. Dorkin, A. Vegas and D. Anderson, *Nature materials*, 2013, 12, 967-977.
8. R. L. Kanasty, K. A. Whitehead, A. J. Vegas and D. G. Anderson, *Molecular therapy : the journal of the American Society of Gene Therapy*, 2012, 20, 513-524.
9. A. M. Bodles-Brakhop, R. Heller and R. Draghia-Akli, *Molecular therapy : the journal of the American Society of Gene Therapy*, 2009, 17, 585-592.
10. H. Aihara and J. Miyazaki, *Nature biotechnology*, 1998, 16, 867-870.
11. G. A. Hofmann, *Methods in molecular medicine*, 2000, 37, 37-61.
12. K. Mori, T. Hasegawa, S. Sato and K. Sugibayashi, *Journal of controlled release : official journal of the Controlled Release Society*, 2003, 90, 171-179.
13. D. J. Wells, *Cell biology and toxicology*, 2010, 26, 21-28.
14. S. Mazeris, D. Sel, M. Golzio, G. Pucihar, Y. Tamzali, D. Miklavcic and J. Teissie, *Journal of controlled release : official journal of the Controlled Release Society*, 2009, 134, 125-131.
15. R. F. Donnelly, T. R. Singh, M. J. Garland, K. Migalska, R. Majithiya, C. M. McCrudden, P. L. Kole, T. M. Mahmood, H. O. McCarthy and A. D. Woolfson, *Advanced functional materials*, 2012, 22, 4879-4890.
16. J. W. Lee, S. O. Choi, E. I. Felner and M. R. Prausnitz, *Small*, 2011, 7, 531-539.
17. Saijilafu, E. M. Hur and F. Q. Zhou, *Nature communications*, 2011, 2, 543.
18. S. O. Choi, Y. C. Kim, J. H. Park, J. Hutcheson, H. S. Gill, Y. K. Yoon, M. R. Prausnitz and M. G. Allen, *Biomedical microdevices*, 2010, 12, 263-273.
19. S. O. Choi, Y. C. Kim, J. W. Lee, J. H. Park, M. R. Prausnitz and M. G. Allen, *Small*, 2012, 8, 1081-1091.
20. D. M. Soden, J. O. Larkin, C. G. Collins, M. Tangney, S. Aarons, J. Piggott, A. Morrissey, C. Dunne and G. C. O'Sullivan, *Cancer letters*, 2006, 232, 300-310.
21. W. Zewen, H. Yuanyu, Z. Deyao, L. Zicai and L. Zhihong, *TRANSDUCERS 2011 - 2011 16th International Solid-State Sensors, Actuators and Microsystems Conference*, 2011, DOI: 10.1109/transducers.2011.5969380, 1942-1945.
22. W. Zewen, W. Renxing, Z. Shuquan, L. Zicai and L. Zhihong, *Micro Electro Mechanical Systems (MEMS), IEEE 27th International Conference on*, 2014, DOI: 10.1109/MEMSYS.2014.6765766, 817-820.
23. V. Ntziachristos, C. Bremer and R. Weissleder, *European radiology*, 2003, 13, 195-208.
24. J. M. McMahon, E. Signori, K. E. Wells, V. M. Fazio and D. J. Wells, *Gene therapy*, 2001, 8, 1264-1270.
25. R. L. Bogorad, H. Yin, A. Zeigerer, H. Nonaka, V. M. Ruda, M. Zerial, D. G. Anderson and V. Koteliansky, *Nature communications*, 2014, 5, 3869.
26. Y. Sakurai, H. Hatakeyama, Y. Sato, M. Hyodo, H. Akita and H. Harashima, *Molecular therapy : the journal of the American Society of Gene Therapy*, 2013, 21, 1195-1203.
27. T. Arif, L. Vasilkovsky, Y. Refaely, A. Konson and V. Shoshan-Barmatz, *Molecular therapy. Nucleic acids*, 2014, 3, e159.
28. F. N. Rasheed, M. Locniskar, D. J. McCloskey, R. S. Hasan, T. J. Chiang, P. Rose, R. de Soldenhoff, H. Festenstein and K. P. McAdam, *Clinical and experimental immunology*, 1989, 76, 391-397.